J. Am. Soc. Mass Spectrom. (2017) 28:2262–2279
DOI: 10.1007/s13361-017-1754-4

RESEARCH ARTICLE

Charging and Release Mechanisms of Flexible Macromolecules in Droplets

Myong In Oh, Styliani Consta

Department of Chemistry, The University of Western Ontario, London, ON N6A 5B7, Canada

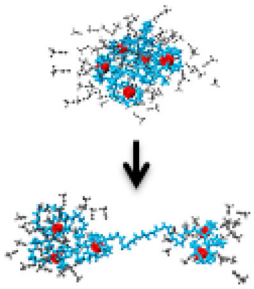

Abstract. We study systematically the charging and release mechanisms of a flexible macromolecule, modeled by poly(ethylene glycol) (PEG), in a droplet by using molecular dynamics simulations. We compare how PEG is solvated and charged by sodium Na^+ ions in a droplet of water (H_2O), acetonitrile (MeCN), and their mixtures. Initially, we examine the location and the conformation of the macromolecule in a droplet bearing no net charge. It is revealed that the presence of charge carriers do not affect the location of PEG in aqueous and MeCN droplets compared with that in the neutral droplets, but the location of the macromolecule and the droplet size do affect the PEG conformation. PEG is charged on the surface of a sodiated aqueous droplet that is found close to the Rayleigh limit. Its charging is coupled to the extrusion mechanism, where PEG segments leave the droplet once they coordinate a Na^+ ion or in a correlated motion with Na^+ ions. In contrast, as PEG resides in the interior of a MeCN droplet, it is sodiated inside the droplet. The compact macro-ion transitions through partially unwound states to an extended conformation, a process occurring during the final stage of desolvation and in the presence of only a handful of MeCN molecules. For charged H_2O/MeCN droplets, the sodiation of PEG is determined by the H_2O component, reflecting its slower evaporation and preference over MeCN for solvating Na^+ ions. We use the simulation data to construct an analytical model that suggests that the droplet surface electric field may play a role in the macro-ion–droplet interactions that lead to the extrusion of the macro-ion. This study provides the first evidence of the effect of the surface electric field by using atomistic simulations.

Keywords: Electrospray ionization, Charged droplets, IEM, CRM, Charge state, Macromolecules, Mixture of solvents, Desolvation, Evaporation, CI-EM, A-CEM

Received: 13 December 2016/Revised: 28 May 2017/Accepted: 29 May 2017/Published Online: 11 August 2017

Introduction

Electrospray ionization (ESI) operates by spraying an aerosol of charged droplets. These droplets are the intermediate carriers that transfer charged macromolecules from bulk solution into the gaseous state. ESI is often coupled to mass spectrometry (MS) for the analysis of chemical and biochemical species ranging in complexity from simple molecules to macromolecular assemblies [1, 2]. In ESI experiments, electrosprayed droplets often comprise solvent, charged macromolecules, and other simple charge carriers. During its lifetime, a droplet disintegrates via solvent evaporation and releases of solvated ions. After a sequence of such dynamic events, the analytes are eventually transferred from the droplet into the gas phase. One of the long-lasting questions in the studies of ESI-MS is to find out the mechanisms through which charged macro-ions emerge from droplets. These release mechanisms have been related to the final charge states of the gaseous macro-ions.

The fundamental model that has been used to understand the fragmentation event of a droplet is the Rayleigh model, developed by Lord Rayleigh [3] in 1882, on the stability of a charged spherical conductor that may undergo shape fluctuations [4, 5]. In the fluctuating shapes, the volume of the droplet is constant but the surface area may change. In the Rayleigh model, linear stability analysis of the total energy of the droplet [4, 6] leads to the Rayleigh limit for the stability of the droplet, which is given by:

$$Q_R^2 = 64\pi^2\varepsilon_0\gamma R_0^3 \quad (1)$$

where Q_R denotes the charge of the droplet at the Rayleigh limit, ε_0 the vacuum permittivity, γ the surface tension, and R_0 the droplet radius. Hereafter we will refer to the droplet being found

Electronic supplementary material The online version of this article (doi:10.1007/s13361-017-1754-4) contains supplementary material, which is available to authorized users.

Correspondence to: Styliani Consta; *e-mail:* sconstas@uwo.ca

"below the Rayleigh limit" when $Q_R^2 < 64\pi^2\varepsilon_0\gamma R_0^3$. When the relation is reversed, the droplet is referred to be found "above the Rayleigh limit". It has been revealed in experiments [7–13] and we have found by molecular simulations [5] that the Rayleigh model predicts well the onset of the charge-induced instability even in the cases where all the charge of the droplet is carried by a single macro-ion solvated in the interior of the droplet [14, 15].

Later, two major mechanisms, the charge-residue model (CRM) [16, 17] and the ion-evaporation mechanism (IEM) [18–20], were developed in the field of ESI-MS in order to address the important question of how the charge state of a macro-ion is related to the mechanism by which it emerges from a droplet. In the CRM, a droplet composed of solvent, single ions and a macro-ion reduces its charge by a sequence of solvent evaporation and solvated ion ejection events at the Rayleigh limit. At the latest stage of the droplet's lifetime when its size is comparable to the size of the macro-ion, complete desolvation collapses the remaining ions onto the macromolecule. This model was formulated by de la Mora [17], and it has been used for explaining the charge of the macro-ion. The IEM was developed by Iribarne and Thomson [18] for single ions escaping from a droplet that is found below the Rayleigh limit. The model describes the activation energy of single ion release in droplets below the Rayleigh limit when ion evaporation rate is higher than solvent evaporation rate. Later, Fenn and co-workers used the IEM, also called the ion-desorption mechanism (IDM), to relate the charge states of a macro-ion with its escape from a droplet.

In 2008, Hogan et al. [21, 22] proposed a combined charged residue-field emission model that predicts the final average charge on proteins. This model determines the charge state of the droplet not by the Rayleigh limit (Equation 1), but by the critical electric field on the droplet surface required for the emission of solvated small ions and protons. A protein that is assumed to be found in the interior of a droplet acquires the charge from the ions remaining in the droplet based on the electric field criterion. The authors reported that their model agrees with the experimental data on the charge states of proteins.

During the last decade, new insights into the disintegration mechanisms of charged droplets have been obtained from computer modeling. Steinberg et al. [23] studied the desolvation mechanism of cytochrome *c* by performing several constant-energy molecular dynamics (MD) simulations on droplets composed of a charged cytochrome *c* and a single solvation shell of water surrounding the protein. The rate of solvent evaporation as a function of temperature and the protein conformations were analyzed. Studies of the structure of several proteins and the effect of solvent evaporation on their conformations have been also performed by Patriksson et al. [24]. Consta [25] identified different droplet states due to the high charge of compact or linear macro-ions. Consta et al. [26] presented the first example of macro-ion extrusion from droplets by molecular simulations of sodiated or lithiated poly(ethylene glycol) (PEG). The extrusion of macromolecules from droplets has been hypothesized by Fenn and de la Mora [17], yet there has not been any direct evidence of the mechanism. To our knowledge, a charged PEG molecule is the only example of extrusion of a realistically modeled macro-ion from a droplet that has been identified up-to-date by molecular simulations. It is highly expected that derivatives of PEG with side hydrocarbon chains or different length of methylene bridges between the oxygen sites will be also extruded from the aqueous droplet; however, this study has still not been performed. The analytical theory in combination with the simulations in Refs. [5, 25–28] showed how the interplay between the solvation energy of a macro-ion and the charge in the droplet determines the mechanism by which a macro-ion emerges from a droplet. The analytical model of the extrusion mechanism of a linear macro-ion from a droplet is presented in Ref. [28], and the generalization of the model for the various manners that a macro-ion may be expelled from a droplet or remain solvated is presented in Ref. [5]. In 2012, an ejection mechanism of a chain was also described by Ahadi, Konermann, and co-workers [29, 30] who used MD simulations to study the effect of hydrophobicity of a bead-spring modeled chain on the mechanistic process in electrospray ionization. The authors reported, however, that their model was not intended to relate to any realistic molecule because of the lack of proper parametrization and structure. A discussion of the model is found in Ref. [5].

In this study, we continue our analysis on understanding the manners in which PEG is released from droplets of water, acetonitrile (MeCN), and their mixtures. Our previous studies have shown that macro-ions induce diverse droplet morphologies above or below the Rayleigh limit that affect the charging mechanisms. The effect of macro-ions on the morphology of charged droplets and their stability has been addressed by Fenn [31, 32] and de la Mora [17] who proposed that the extension of the macro-ion is caused by Coulomb repulsion and, as a result, the droplet becomes elongated with conical ends that accumulate the charge density. Although previous suggestions as to how droplet morphologies influence macro-ion charging have been insightful, it is only in the last decade that a direct observation of the droplet morphologies and their relation to the charge states is possible via the use of atomistic simulations.

The variety of the droplet morphologies implies that the droplet structure may affect the charge state and the conformation of a macro-ion and the stability of complexes of macro-ions (for instance, nucleic acids and protein complexes) in a distinct manner relative to those in the spherical droplets and the bulk solution [14, 15]. The droplet morphologies and their effects cannot be captured at the molecular level by the conventional CRM and IEM or the model proposed by Hogan et al. [21, 22]. The release of a macro-ion from a droplet is a far more complicated process than that of simple ions because of the complexity in the structure of the macro-ion and the chemical modifications that it may undergo in relation to its release. Because of this complexity, we have proposed two mechanisms: (1) the CI-EM (charging-induced extrusion mechanism), which takes into account the role of the chemical modifications of the macro-ion in its extrusion mechanism [5, 26, 27, 33], and (2) the A-CEM (activated-contiguous extrusion mechanism), which considers that the macro-ion is already

charged (there are no chemical modifications of the macro-ion that are coupled to the release mechanism). Detailed descriptions of those mechanisms are found in Refs. [5, 28].

PEG has a persistence length of 3.7–3.8 Å [34, 35]. Its persistence length is small relative to the contour length of the specific PEG64 (64 denotes the number of monomers) that we examine, which is approximately 275 Å; thus the PEG molecule represents a flexible macromolecule. We selected to study the sodiation of PEG because (1) our previous research has shown that the interactions of PEG with water and Na^+ ions can be modeled reliably with the existing force fields [26, 27, 33]; (2) we can directly and realistically study the coupling between the charging of PEG and its release mechanisms from droplets [5, 33]; (3) PEG–ion interactions have been extensively studied experimentally by the methods of mass spectrometry [17, 36–41].

In the present study, we compare neutral to charged droplet systems in the presence of the macromolecule. Our key findings are: (1) In water, PEG is localized onto the droplet surface where its segments capture Na^+ ions and extrude into the vapor phase via the CI-EM. In MeCN, in contrast, PEG resides inside the droplet, eventually emerging in the vapor phase (with bound Na^+ ions) after nearly all MeCN has evaporated away. (2) The different solvent–PEG interactions determine the final charge state and thus the conformation of PEG. Almost always PEG64-$4Na^+$ is found to be extruded from an aqueous droplet, whereas PEG64 bound to fewer than four Na^+ ions is the most probable outcome from an MeCN droplet. Depending on the final charge state, the released macromolecule is compact, partially stretched, and extensively stretched [26]. Interestingly, at the latest stage of droplet desolvation, a few MeCN molecules suffice to maintain the charged macromolecule compact. (3) Although PEG displays distinct behavior of solvation and sodiation in droplets of pristine H_2O and MeCN solvents, when PEG is in a droplet composed of a binary mixture of the two solvents, the final charge state is almost always four as in a pristine water droplet. We found that this is attributed to (a) the preferential solvation of Na^+ ions in water and (b) the aqueous core formation due to differential solvent evaporation of water and MeCN. Moreover, based on our simulation data, we construct an analytical model that suggests that the droplet surface electric field may play a role in the macro-ion–droplet interactions that lead to the extrusion of the macro-ion. Although the role of the surface electric field has been suggested previously [18, 19], here we provide the first evidence of the effect of the surface electric field via molecular simulations with atomistic details.

Model and Computational Methods

Modeling of the Interatomic Interactions

We performed molecular dynamics (MD) simulations of droplets composed of solvent, a poly(ethylene glycol) molecule with 64 monomers (PEG64), and Na^+ ions. The solvent was selected to be H_2O, MeCN, and a mixture of H_2O/MeCN with various compositions. These solvents are commonly used in ESI-MS experiments. PEG was chosen as a realistic model for a flexible linear macromolecule, and Na^+ ions were used as simple charge carriers to render the droplet excess positive charge. The PEG and MeCN molecules were modeled using the OPLS-AA (Optimized Potential for Liquid Simulations - All Atom) [42, 43] force field where all hydrogen atoms are explicitly represented. The OPLS-AA force field includes optimized potential terms for bond-stretching and angle-bending vibrations, which are described by an ideal harmonic oscillator, as well as torsional strains, Coulombic electrostatic interactions, and Lennard-Jones (LJ) interactions. The PEG molecule was terminated with methyl groups. The parameters for the atomic sites of the PEG molecule were taken from those for ethers. The water molecules were represented by the TIP3P (three-site transferable intermolecular potential) model [44]. All the MD simulations were carried out by using the GROMACS [45] version 4.5.5 molecular simulation program. The Visual Molecular Dynamics (VMD) [46] software was used for the purpose of all visualizations.

System Modeling and Simulation Set-up

Detailed information of the different parameters used in building systems and running simulations is summarized in Supplementary Table S1 in the Online Resource.

Neutral Droplets PEG64 was solvated in H_2O and MeCN droplets with varying sizes (250–7000 H_2O molecules and 250–1500 MeCN molecules). Equilibrium runs were performed by placing the droplet system into a cubic simulation box with periodic boundary conditions (PBC). The size of the simulation box was approximately three to four times larger than the diameter of the droplet so as to ensure that the system does not interact with its images and to allow for the shape fluctuations of the droplets. The temperature was set at 300 K and 250 K for water and MeCN droplets, respectively, so that vigorous solvent evaporation was suppressed. The time step of integration was set to 1 fs. in all the runs. MD was performed using the leap-frog algorithm and the temperature was maintained by velocity rescaling. The long-distance electrostatic and van der Waals interactions between non-bonded atoms were truncated using the switch function. In this scheme, the Coulomb and LJ potential functions are decreased over the entire range, and the forces decay smoothly to zero between the switch and the cutoff radius, so that the forces and their derivatives are continuous at the cut-off radius. The switch distances employed for 250 H_2O, 800 H_2O, 1500 H_2O, 4000 H_2O, and 7000 H_2O were 4.0 nm, 5.0 nm, 5.5 nm, 7.5 nm, and 9.0 nm, respectively. Those for 250 MeCN, 800 MeCN, and 1500 MeCN were 4.5 nm, 6.5 nm, and 8.0 nm, respectively. The cut-off radii were 1 nm longer than the corresponding switch distances.

The simulations were prepared with different initial conditions where either a compact or stretched conformation of PEG64 was

initially placed inside the droplets for the aqueous droplets with more than 250 H_2O molecules. Furthermore, four additional aqueous droplets consisting of 4000 water molecules and PEG with 30, 40, 50 and 64 monomers were simulated at the same conditions as described above for 4 ns, so as to test the location of PEG in the droplets. In these systems, a compact PEG was initially solvated inside the aqueous droplets. A simulation of PEG64 in vacuo without any solvent was also performed for 100 ns for the purpose of comparisons with the other systems.

Charged Droplets For every charged droplet system, constant-temperature MD simulations were performed using the leap-frog algorithm and velocity rescaling to thermostat and maintain the desired temperature. The time step of integration was set to 0.5 fs. in all the runs, and electrostatic and van der Waals interactions were not truncated. Each droplet system was placed in vacuo without the PBC, allowing non-equilibrium runs where solvent and ion evaporations were allowed. Droplets reduced in size by solvent evaporation and Coulomb fission during the simulations. The evaporated molecules and ions were removed when they were found at a distance longer than three times larger than the diameter of the droplet from the connected body of the system.

Aqueous Droplets A stretched PEG64 was initially solvated in a cubic solvent box constructed with 7000 water molecules. Several water molecules were replaced with Na^+ ions in order to introduce excess positive charge into the system. Three different numbers of the ions (16, 32, and 128 Na^+) were implemented. The temperature was set at $T = 300$ K. Details of these simulations are also found in our previous study [33].

MeCN Droplets Four charged droplets, each composed of 800 MeCN molecules, one PEG64 molecule and Na^+ ions (N_{Na^+} =2, 4, 8, and 12), were prepared and simulated. For the purpose of comparison, an electrically neutral droplet of MeCN (i.e., $N_{Na^+} = 0$) was also simulated. The initial conformation of the PEG64 molecule in the droplets was compact, which was obtained from the simulation of a bare PEG64 molecule in vacuo. In order to investigate the effect of temperature on the charging mechanism of the macromolecule in the MeCN droplets, we varied the temperature; the systems evolved under four different temperatures (namely, 250 K, 280 K, 300 K, and 320 K) which are all lower than the experimental boiling point of bulk acetonitrile (≈355 K) [47]. By visual inspection, we inferred that only the pure MeCN droplet charged with +12 *e* is above the Rayleigh limit at $T = 280$ K as it undergoes immediate fissions at the very early stage of the realization. Additionally, in order to study the effect of solvation on the conformational size of the macromolecule, a PEG64 with the maximum number of Na^+ ions that can attain, which is five (PEG64-5Na^+) [48], was solvated inside a MeCN droplet and simulated at $T = 280$ K.

H_2O/MeCN Droplets Five different solvent compositions with mole fractions of MeCN (χ_{MeCN}), ranging from χ_{MeCN} = 0 (corresponding to pure H_2O) to χ_{MeCN} = 1.0 (corresponding to pure MeCN), were examined. The total number of the solvent molecules and the amount of Na^+ ions were maintained identical at the initial setup for every system ($N_{solvent}$ = 800, $N_{Na^+} = 8$). The temperature was maintained approximately at 280 K.

Results and Discussion

Neutral Systems

Macromolecules on the Surface of the Droplet Typical snapshots of the solvation of PEG64 in aqueous droplets of various sizes are shown in Figure 1a–c. In all the systems at equilibrium, PEG consistently resides on the surface of the droplets. The statistical sampling of the PEG location was tested by preparing ten initial configurations where the PEG64 was well solvated in the interior of the droplet. Among these configurations, droplets of 4000 water molecules with PEG30, PEG40, PEG50, and PEG64 were simulated, starting from PEG at the center of the droplet. In all the systems, the PEG phase-separated from the aqueous droplet within 4 ns. We found that there was no obvious correlation between the length of PEG and the diffusion time. It is interesting that the PEG64 does not entirely adhere to the surface of the droplet; rather, it often forms multiple loops that alternate between regions immersed into the solvent and regions detached from the water/vapor interface of the droplet. These alternating loops are shown in the inset of Figure 1c. The loops are dynamic and the time scale that a segment of PEG64 is immersed into the droplet may vary from several tens of picoseconds to a few hundreds of picoseconds. The alternating loops of PEG have been consistently found at the water/vapor interface in modeling performed by Prasitnok et al. [49]. In those studies, coarse-grained modeling of multiple PEG chains was performed in the liquid/vapor interface of an aqueous solution.

The conformations of PEG64 were quantified by measuring the radius of gyration (R_g) and the end-to-end distance (R_{EE}) of the polymer. The histograms of the R_g and R_{EE} distributions are shown in Figures 2b and S1 in the Online Resource, respectively. The most probable values of R_g and R_{EE} converge to an upper limit as the droplet size increases. The convergence of the most probable values of R_g and R_{EE} with increasing the droplet size can be also demonstrated by plotting these values versus the number of H_2O molecules (N_{H_2O}) in a droplet (Figure S3 in the Online Resource). This limit should be close to the chain dimensions observed in the case of a bulk water/vapor interface.

To find the origin of the convergence of the R_g and R_{EE} distributions, the maximum number of solvent molecules in the first solvation shell of PEG64 and the droplet curvature (κ)

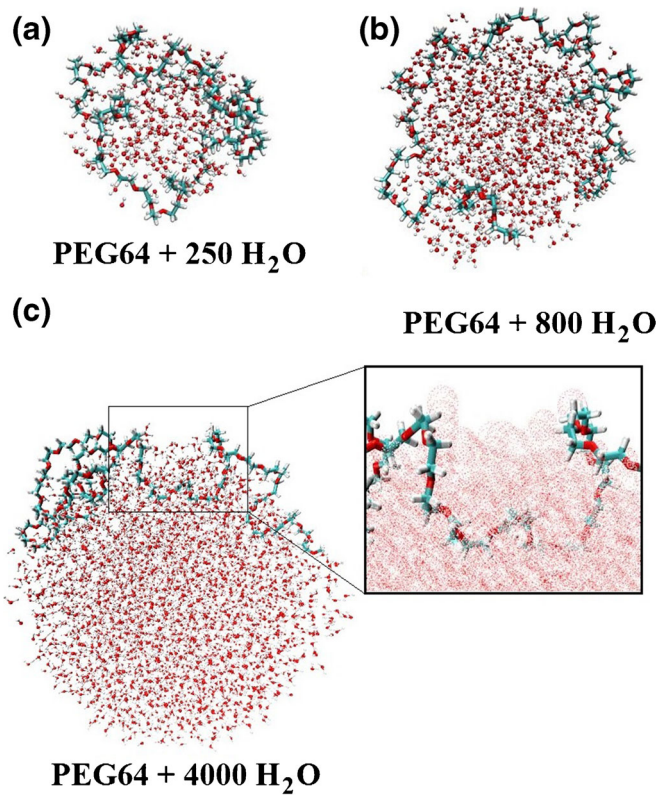

Figure 1. Typical snapshots (**a**)–(**c**) of aqueous droplets of various sizes that contain a PEG64 molecule. The inset of (**c**) shows the magnification of a region of (**c**) that shows the alternating loops in and out of an aqueous droplet of 4000 H_2O molecules. The H_2O molecules are represented by dotted red spheres

versus the number of the H_2O molecules in the droplet were examined. Figure 2a shows a rapid increase in the number of water molecules in the first solvation shell of PEG64. This maximum number is attained when the number of the solvent molecules is 1500 or more. This convergence indicates that the maximum solvent–monomer interaction sites have been saturated for the polymer at that location; in other words, there is an upper limit of the contact area available for the interaction with the solvent. As shown in the inset of Figure 2a, assuming that the droplet is in a spherical shape, the curvature of the great circle decreases and converges to a value close to zero in the same manner as the number of water molecules in the first solvation shell of PEG converges. When the diameter of the droplet is relatively large (≈7 nm), the curvature comes close to zero and the droplet surface mimics the flat surface of a solvent/vapor interface. The change of the slope in the curvature of the droplet and the maximum interaction contacts of PEG64 with H_2O versus the droplet size is in agreement with that of the R_g and R_{EE} values. All the quantities show the onset of the convergence at approximately 1500 H_2O molecules (which correspond to a droplet with diameter D of ≈4.7 nm), and they clearly reach a plateau at approximately 4000 H_2O molecules (D≈6.9 nm). The convergence of these quantities with the size of the droplet is greatly affected by the curvature of the droplet because of the location of the PEG on the surface and its specific interactions with the solvent at the droplet/vapor interface.

Macromolecules in the Interior of an Acetonitrile Droplet

Differently from PEG64 in aqueous droplets, it is consistently observed that the macromolecule settles in the interior of the MeCN droplets. Typical configurations of the droplets are shown in Figure S4 in the Online Resource.

In general, the preferential location of PEG64 on the surface versus in the interior of droplets of various solvents has its roots in the relative strengths between solvent-monomer and solvent–solvent interactions. The complete solubility of PEG in water and many organic solvents such as MeCN, MeOH, benzene, and chloroform has been widely recognized experimentally [50, 51]. MeCN molecules lack the hydrogen-bonding ability, and therefore, it is dipole–dipole interactions that prevail for solvent–solvent and solvent–monomer interactions. The lack of the ability to form strong hydrogen bonds between PEG and MeCN may be compensated by the high dipole moments of the individual solvent molecules. Hakem and Lal [51] computed the solubility parameters of PEO in H_2O and MeCN solutions at room temperature by applying the Hildebrand equation, and they expected lower polymer solubility in MeOH than in MeCN. In our previous study [33], we found that PEG resides inside a MeOH droplet, regardless of the presence of charge carriers. Moreover, MeCN molecules share a common methyl group that water molecules do not possess. These two factors (i.e., the similarity in the structure and the intermolecular interactions) may cause the solvation of PEG in the interior of MeCN droplets.

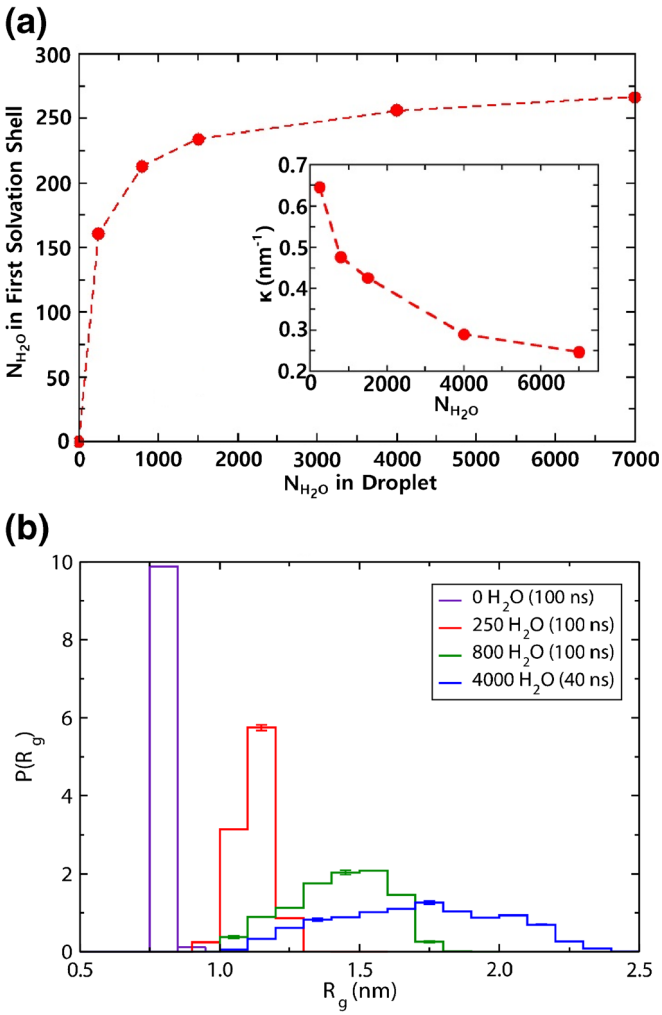

Figure 2. (**a**) Number of H_2O molecules in the first solvation shell of PEG64 as a function of the droplet size. The inset shows the change in the droplet curvature (κ) versus N_{H_2O}. (**b**) Probability density (P) of the radius of gyration (R_g) of PEG64 in aqueous droplets of various sizes. The length of the production run is indicated in the legend and the bin size is 0.1 nm

Since PEG64 lies in the interior of the droplet, we conjecture that its dimensions are affected largely by the diameter of the droplet. We center the following discussion around MeCN: Figure S2 in the Online Resource shows the R_{EE} and R_g distributions of PEG64 in MeCN droplets as a function of the droplet size. The R_{EE} and R_g distributions reveal the strong correlation of the conformational dimensions to the size of the hosting droplet. In addition, their fluctuations also increase with the size of the droplet, implying more conformational freedom granted to the polymer simply due to more physical space available to it. In MeCN, the dimensions of PEG64 with respect to the number of solvent molecules converge faster than those observed in H_2O.

The convergence of PEG64 dimensions to an upper limit is in agreement with the findings of Cifra et al. [52], who demonstrated that the mean R_{EE} and R_g of a polymer in a spherical cavity converge to an upper limit as the sphere radius increases. The same trend was observed for polymers with different stiffness parameters [52]. In those simulations, a hybrid coarse-grained model of semi-flexible chains was employed, which comprises bead units and stiff springs for effective bonds. The sphere restricts the motions of the monomers in all directions when its size is quite small compared to the size of the macromolecule, yet when the radius is fairly large, it can mimic the bulk environment. The confinement effect exerted by the droplet's finite size on the dimensions of the macromolecule is a general feature that is consistent with the findings of other theoretical studies of the effect of a cavity on polymer dimensions [52–59].

In summary, the strong droplet-size-dependent conformational dimensions of PEG64 and their convergence to an upper threshold are common features in the solvents of water and acetonitrile. These findings indicate that the confinement effect is not solvent-specific, and it is completely independent of the location of the macromolecule in a droplet. The confinement effect manifests itself in the most probable values of R_g and R_{EE} and the extent of their fluctuations. We found that the most probable R_g and R_{EE} of PEG64 in water droplets decrease by approximately 50% and 70%, respectively, as the radius of the droplet decreases from 3.8 nm to the zero solvent molecules (i.e., dry PEG64 conformation). Also, in MeCN droplets, PEG64

shows a decline in the most probable R_g and R_{EE} values, approximately by 39% and 12%, respectively, as the radius of the droplet drops from 3.2 nm to zero. The transition from the extended conformation of PEG64 in larger droplets to the dry state is continuous. Because of the convergence in the most probable values of R_g and R_{EE} in droplets with radius larger than 3.3 nm and 3.2 nm for water and MeCN, respectively, we demonstrated that the droplet confinement plays a role in droplets with radius smaller than 3.2 nm. When PEG64 is close to dryness, the confinement effect diminishes.

Charging of a Macromolecule in Pure Solvent Droplets

Macromolecule on the Surface of a Water Droplet The charging mechanism of a flexible linear macromolecule, modeled by PEG in aqueous droplets, has been discussed in our previous articles [26–28, 33, 48, 60]. For the sake of completeness, here we summarize our previous findings, but we also provide new insight regarding the charging mechanism. The discussion is about the sodiation of PEG64 in an aqueous droplet, but the findings are not limited to this particular length of PEG and type of ions [27]. In our previous studies, we simulated the sodiation of PEG of various lengths in droplets of 7000 H_2O molecules (approximate radius of 4 nm) down to several hundreds of H_2O molecules (approximate radius of 1 nm) [33, 48] at temperatures ranging from 280 K to 350 K. The results presented here are from simulations performed for this article for PEG64 in aqueous droplets at $T = 300$ K. We found that, regardless of the contour length and the initial configuration of the macromolecule and the nature of the charge carriers [27], PEG settles on the surface of the droplet. The strong hydrogen-bonding network formed by water molecules determines the interfacial confinement of the macromolecule [49, 61–64].

We found that the sodiation of PEG takes place at the liquid/vapor interface of the droplet, and it is coupled to its escape from the droplet [33]. Typical snapshots of the charging of PEG64 during the course of solvent evaporation are shown in Figure 3. This simulation started from a droplet of approximately 6500 H_2O molecules with 16 Na^+ ions and PEG64 (Figure 3a). These system parameters correspond to a charge-squared-to-volume ratio of the droplet considerably below the Rayleigh limit. The release of the sodiated PEG from an aqueous droplet is the result of a series of chemical events. The sodiation of PEG does not occur at any droplet size, but at a droplet size that reaches a critical Na^+ concentration. This concentration is approximately that of 20 Na^+ ions in a droplet of 6500 H_2O molecules as it was found in our previous simulations [33] or higher. In Figure 3b, the first sodiation occurs when 16 Na^+ ions remain in approximately 3500 H_2O molecules. When a Na^+ ion is captured by PEG64, it becomes coordinated by the oxygen sites of the monomers (Figure 3b). The PEG segment that encloses the Na^+ ion exposes its hydrophobic methylene group toward the aqueous surface, resulting in weaker interactions with the solvent molecules present at the droplet surface. Once one sodiated segment of PEG is released, it remains extended at an equilibrium position. To a first approximation, this position is determined by the balance between the solvation force and the electrostatic repulsion. In the next section, we analyze the equilibrium in the extended segment in order to obtain insight into factors that play a significant role in the solvation energy. This cycle of sodiation and partial releases repeats until PEG64 is charged with four Na^+ ions and then it is completely detached from the parent droplet. The sodiated segment can easily detach from the droplet as shown in Figure 3c, d. Previous simulations [26, 27] and analytical theory [5] have shown that depending on the amount of remaining charges in the droplet, a sodiated PEG may entirely leave the droplet or stay partially attached to the droplet and dry out.

We found two mechanisms via which the aqueous droplet reduces its excess charge when it is close (from below) to the Rayleigh limit. (1) A Na^+ ion is released by first attaching to PEG (Movie S1 in the Online Resource). The attachment of the Na^+ ion onto PEG can occur directly by the transfer of the cation from H_2O into PEG, where it is wrapped by the ethereal oxygen sites at the surface of the droplet first, and then it is released along with the PEG portion. Our simulations also revealed that when a Na^+ ion is located in proximity to PEG, it may be released as a small droplet without initially being wrapped by the macromolecule. The solvated Na^+ ion keeps in contact with PEG as it detaches from the droplet, and it drags a short segment of the PEG with it. Then, the solvated ion rolls on the extruded part of the PEG until the ion is eventually wrapped by PEG when the water shell around the Na^+ ion completely dries out. (2) The cation escapes the parent droplet simply by a release from the surface of the droplet that is not occupied by PEG (Movie S2 in the Online Resource). For large droplets, it was found that Na^+ (or $Na(H_2O)_n^+$) emission from the surface occurs rarely compared to Na^+ transfer to PEG within the droplet. The escape of an ion from a conductor such as an aqueous droplet with Na^+ ions is expected to be an activated process because of the induced charge on the conductor. However, in the release of the sodiated segments of PEG, this activation barrier appears to be lower than the release of a water-solvated ion. This is evidenced by the fact that for a certain charge-squared-to-volume ratio in the droplet, we rarely observe the release of the water-solvated ion relative to the PEG-coordinated ion. The ion in PEG is surrounded by a hydrophobic sheath that facilitates its release. In principle, one can estimate from the simulations the activation energy by finding the rate of the escape of the water-solvated and PEG-coordinated ions.

The radius of the droplet remains approximately constant throughout the sodiation and release of PEG. As shown in Figure 3b–d, only ≈8% of the water molecules evaporate during the charging and release of the PEG. In summary, the mechanism that we observe by the example of PEG is the following: the PEG is sodiated in a step-wise process, and the sodiated segments are released faster (due to lower activation energy) than the water-solvated Na^+ ion release. The study of the charging of PEG reveals the charging-induced extrusion mechanism, which we have abbreviated as the CI-EM [5]. In

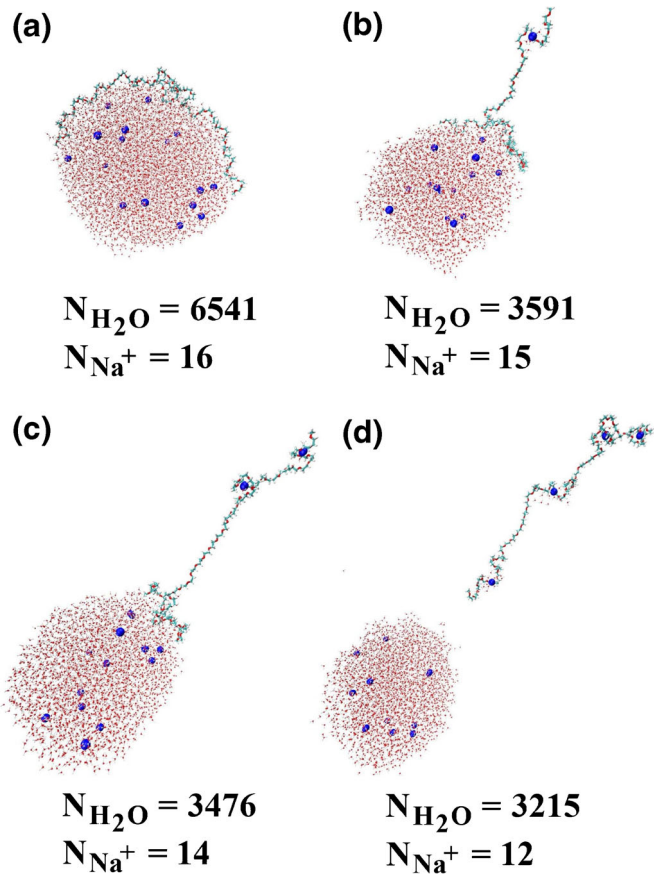

Figure 3. Typical snapshots of PEG64 sodiation and ejection from a charged aqueous droplet. The Na^+ ions are represented by blue spheres. The numbers of water molecules and free Na^+ ions remaining in the main droplet are shown. The duration of the process shown is approximately 65 ns at $T = 300$ K

our previous research, we have developed an analytical model, the activated-contiguous extrusion model (A-CEM) [5, 28] for the extrusion of a linear macro-ion from a conducting droplet. In the A-CEM, the charge density along the macromolecule is constant and is assigned from the beginning. Thus, the effect of the chemical transformations of the macro-ion is not considered. In the A-CEM, the extrusion of the macro-ion is coupled to the reduction of the droplet size due to evaporation. In the phase diagram of the macro-ion extrusion that we have presented in previous research [28], the extrusion occurs along an isoline of the dimensionless parameter expressed by the ratio of the solvation energy to the charge density squared of the macro-ion. Within this model, it may be possible to also describe the CI-EM process by considering jumps on different isolines as the charge density on the macro-ion increases by capturing the Na^+ ions.

It is worth mentioning that expulsion of a non-solvated charged molecule has been deduced by experimental measurements in rhodamine 6G from methanol droplets [65]. In the article, the fluorescence spectra suggest that the extrusion of Rhodamine 6G follows the ion evaporation mechanism (IEM) because the molecules are detected either as completely solvated within the parent droplet or bare of solvent in the gaseous state (i.e., there are no intermediate solvated states). We note that this release mechanism is different from the extrusion of the sodiated PEG. The release of the ionized Rhodamine 6G is similar to the release of a simple ion in contrast to the release of the sodiated PEG, which is a chemically driven multi-step process.

Electrostatic Model of Extrusion We use the simulation data of the extrusion of a charged PEG in combination with analytical modeling to obtain insight into the solvation energy of an extruding linear macro-ion from a droplet. Even though we use the example of an extruding sodiated PEG from an aqueous droplet in the discussion, the reasoning can be applied to other extruding macromolecules as well. The total energy of the system in this analysis is considered to be the sum of its electrostatic and solvation energies. We used the method of images with the underlying assumption that the droplet is a spherical conductor.

In a typical run (e.g., Movie S1 in the Online Resource), one observes droplet-chain configurations where a partially extruded PEG64 persists for several hundreds of picoseconds. The first extruded part carries a single Na^+ ion (Figure 3). We denote by q the charge carried by the extruded portion of PEG64. The parameters of the model

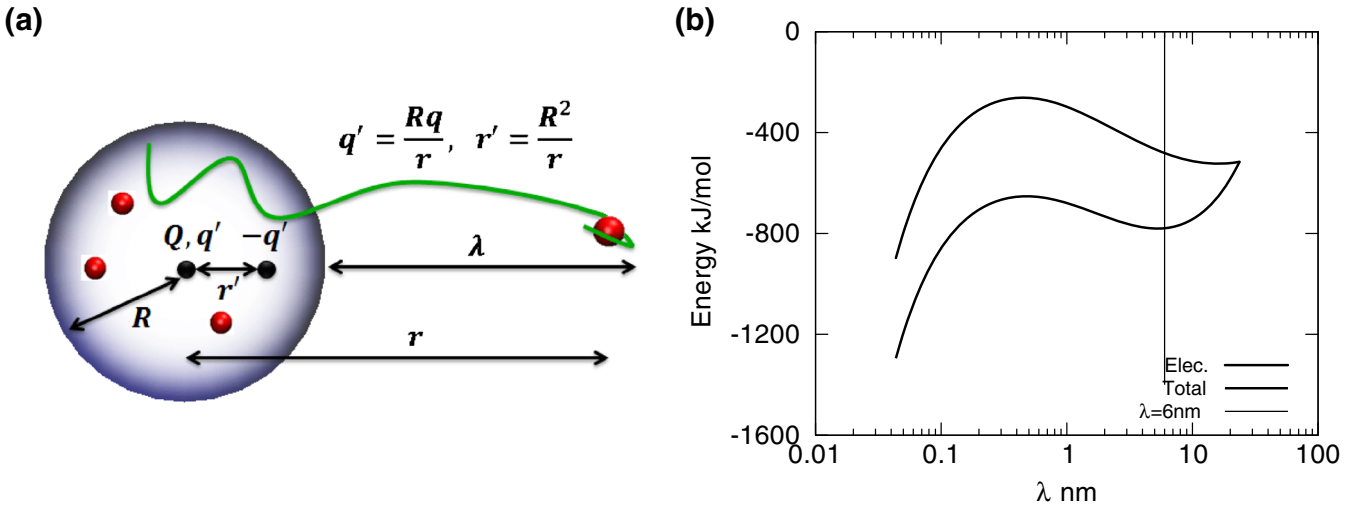

Figure 4. (**a**) Schematic picture that shows the parameters used in the model. The small red spheres and the large blue sphere represent the cations placed randomly and the main droplet, respectively. The green line represents a linear flexible macromolecule. *R* and *Q* denote the radius and the net charge of the droplet, respectively; λ is the length of the extruded portion of the macro-ion; $q^{'}$ is the image charge, whereas $-q^{'}$ is the counter-charge; $r = R + \lambda$ is the distance between the center of the droplet and the cation attached to the macromolecule, and $r^{'}$ indicates the distance of $q^{'}$ from the center of the droplet. (**b**) Energy of extrusion of a linear macromolecule from a spherical conductor. The solid line corresponds to the electrostatic contribution given by Equation **2** of a single charge removal from a conducting sphere with $Q = +8\,e$, and $R = 2.1$ nm. The dashed line is the sum of the electrostatic and solvation energy contributions for the extrusion of PEG64 from a sodiated aqueous droplet. The dotted vertical line marks the 6 nm extension of the PEG64 from the charged droplet found in simulations. Details of the parameters are presented in the text

are shown in the schematic in Figure 4a. The electrostatic energy (W^e) of a spherical conductor of radius R and an extruded charge at a distance $r = R + \lambda$ from the conducting sphere is given by the following equation:

$$W^e = \frac{1}{8\pi\varepsilon_0}\left[\frac{(Q+q')Q}{R} + \frac{(Q+q')q}{r} - \frac{q'q}{r'-r'}\right] \qquad (2)$$

where $q^{'} = Rq/r$ and $r^{'} = R^2/r$ are the magnitude and the position of the fictitious "image" charge, respectively. The radius of the sphere (droplet) is computed from the total volume comprising the water and the solvated part of the chain. The system parameters used to generate the plots in the modeling are presented in Supplementary Table S3 in the Online Resource.

In Figure 4b, we plot the electrostatic energy (solid line) using Equation 2 and the total energy (dashed line), which is the sum of the electrostatic energy (Equation 2) and the solvation energy as a function of λ. In the plots, $Q = +8\,e$, $q = +1\,e$ and $R = 2.1$ nm, which is the radius of a droplet of 1325 H_2O molecules. In Figure 4b, the first minimum approaches minus infinity for a spherical conductor, which implies that the barrier is infinite. In Equation 2 the singularity in the energy is caused by the third term when $r - r^{'} \approx 0$. This singularity is found in the theoretical expressions of the electrostatic energy of a conductor interacting with a charge but simulations have shown that it is unphysical for the release of ions from droplets. The free energy barrier is finite and this is attributed to the shape fluctuations of the droplets.

For the macromolecule with length L, we model the solvation energy by $(L - \lambda)v$, where v is a constant. The discussion of this form of the solvation energy is given in Refs. [5, 28]. In the simulations, we observed a steady state when the chain was extended 6 nm from the droplet surface. This corresponds to 16 out of 64 residues leaving the droplet (Supplementary Table S3). In Figure 4b, the dotted vertical line marks the 6 nm extension of the PEG64 from the charged droplet found in simulations. By minimizing the total energy $(W^e + (L - \lambda)v)$ at $\lambda = 6$ nm, one finds the value of the solvation parameter $v = 16.8\,\mathrm{kJ/nm{\cdot}mol}$. Using this value, the total energy (dashed line) shown in Figure 4b is estimated. The existence of the barrier shows that the escape of a charge from the conducting sphere is an activated process.

Owing to the interaction with an induced charge distribution, in the quasi-static approximation, the interaction energy of the charge with the droplet next to the surface is dominated by the term $-q^2/16\pi\varepsilon_0\lambda$. As the distance from the droplet increases, the electrostatic (repulsion) energy between the droplet and the charge, $Qq/4\pi\varepsilon_0(R + \lambda)$, overcomes the attraction with the image charge. We investigate whether a single constant parameter for the solvation energy can quantitatively explain the chain extrusion from a droplet.

To a first approximation, the electrostatic force exerted on the chain is

$$F = \frac{qQ}{4\pi\varepsilon_0(R+\lambda)^2}. \qquad (3)$$

Because of the balance of the forces in the metastable state of the extruded segment, the electrostatic force equals the solvation force $(\partial(L - \lambda)v/\partial\lambda = -v)$. In Figure 5a, we evaluate the

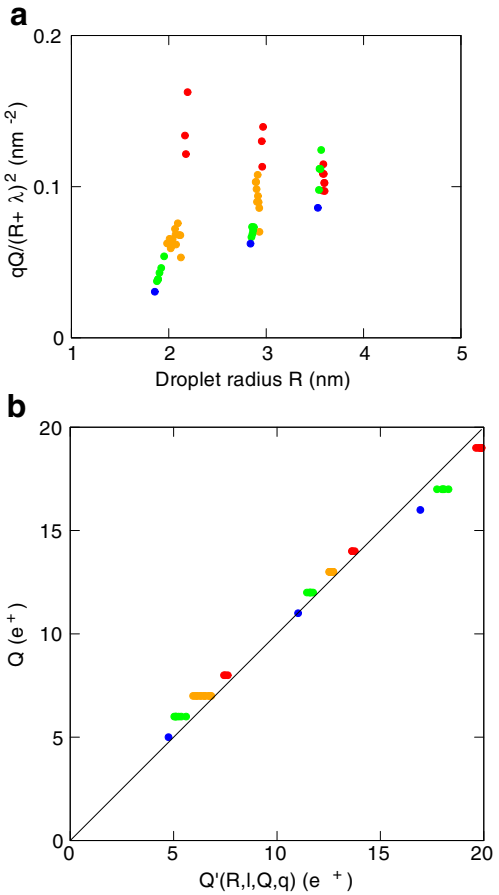

Figure 5. (**a**) Droplet-chain electrostatic force in a united charge approximation explained in the text. Points are color-coded to indicate the charge on the chain. Chain charges q are +1 e (red), +2 e (orange), +3 e (green), and +4 e (blue). (**b**) Fit of the data from (**a**) using a correction to the solvation constant proportional to the magnitude of the electric field on the droplet surface. The points follow the same color scheme as in (**a**)

dependence of the force on the parameters of the system. In the calculations presented in Figure 5a, we use a united charge approximation. In this approximation, we assume that all the charge ($+1\,e$, $+2\,e$, $+3\,e$) is located at the end of the chain. The simulations of the ejection of the PEG molecule have demonstrated a non-uniform charge distribution along the chain. We have observed that in the majority of the simulations all the charges are clustered towards the end of the chain. Hence, to correctly reproduce the electrostatic energy, we used the united charge approximation. Within this model, the points shown in Figure 5a should fall in a horizontal line (constant value). Instead, the values differ considerably. For instance, for a droplet with 1300 water molecules (the leftmost group of points), the values of the electrostatic force vary by an order of magnitude. Therefore, this model may not capture the major components in the total energy of the system. In the next step of the analysis, we hypothesized an additional term in the total energy, which is proportional to the electric field on the surface of the droplet.

We led to this term by the simulation findings. Our simulations show that the macromolecule lies on the surface of the droplet. We expect that the local structure of the water on the surface affects the solvation of PEG64 residing on the droplet surface. We expect that the local structure of the solvent on the surface will depend on the magnitude of the electric field

$$E = \frac{Q}{4\pi\varepsilon_0 R^2}. \tag{4}$$

We test this assumption by using the linear least square fit of the following model

$$-\nu + A\frac{Q}{4\pi\varepsilon_0 R^2} = \frac{qQ}{4\pi\varepsilon_0 (R+\lambda)^2} \tag{5}$$

where ν and A are the fitting parameters. The parameter ν gives the value for the solvation energy per unit length of the chain. In Figure 5, we show the results of the fit in the modified set of parameters $\left(Q, Q^{'}(l,R,Q,q)\right)$ where

$$Q'(l,R,Q,q) = \frac{R^2}{A}\left[4\pi\varepsilon_0\nu + \frac{qQ}{(R+\lambda)^2}\right] \tag{6}$$

Using R statistical analysis software, we obtained the following values for the parameters $\nu = 0.46 \pm 0.03$ and $A = -0.19 \pm 0.02$. The analysis shows that there is a correlation between the electric field on the surface of the droplet and the electrostatic force between the charged extruded segment of the chain and the charged parent droplet. This indicates that the value of the electric field on the surface is potentially connected to the solvation energy. We note that the field we referred to is the one prevailing after an equilibrium is established between neutral evaporation and charge evaporation. The change in the droplet size between PEG charging events is small. The dynamics of the order parameter that corresponds to the degree of chain extrusion is the slowest process compared with the other molecular processes in the system, such as chain conformation dynamics and diffusion of free ions and water molecules. Hence, we consider the solvation force and the electric field to be those of an equilibrated system.

Charging in the Interior of a Droplet We have found that PEG64 is confined in the interior of a MeCN droplet. The presence of simple charge carriers such as Na^+ ions does not affect the preferential solvation of PEG at the center of the droplet relative to the neutral MeCN droplet. Consequently, PEG64 is charged with Na^+ ions inside the droplet. Typical snapshots of the charging of PEG in the interior of an MeCN droplet are shown in Figure 6. Unlike the sequential partial releases of the macro-ion found in a charged aqueous droplet, the MeCN droplet reduces excess charge only through the releases of solvated ions. Hence, the macro-ion emerges from the parent droplet by solvent drying-out. The final charge state of the macromolecule is

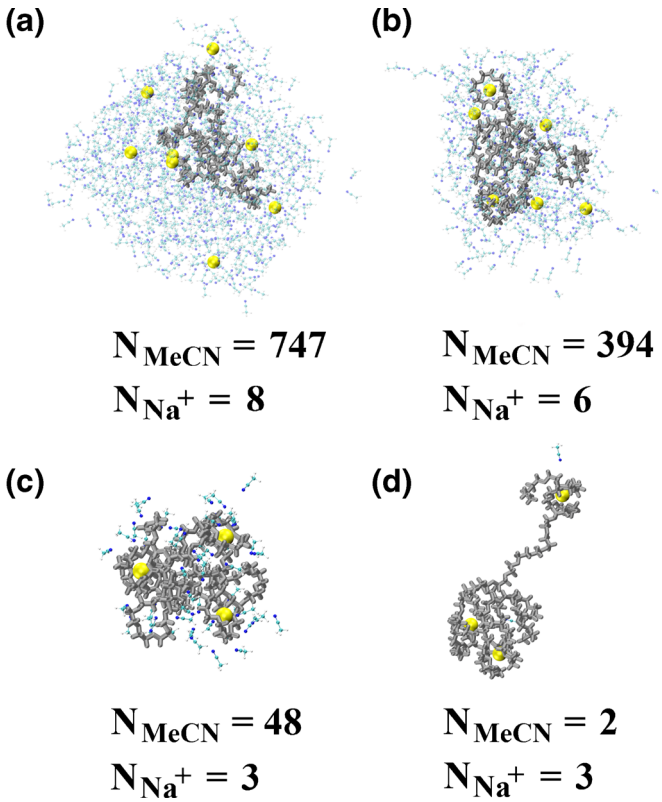

Figure 6. Typical snapshots of PEG64 sodiation and release from a charged MeCN droplet. The Na^+ ions are represented by yellow spheres. PEG64 is colored in gray. For the purpose of better visualization, the molecular details of PEG64 are not shown. The numbers of MeCN molecules and Na^+ ions remaining in the parent droplet are indicated. The duration of the process shown is approximately 10 ns at $T = 280$ K

found to be two or four elementary charges. We have found that the maximum charge state of PEG64 is +5 *e* and it was obtained in aqueous droplets at $T = 273$ K [48]. We found that in MeCN droplets, the initial concentration of the cations and the temperature of the system are significant factors that determine the final charge state of the macromolecule. For instance, at $T = 280$ K, PEG64 obtains a higher charge state (i.e., +3 *e*) when the droplet initially contains more cations (i.e., +8–12 *e*). In droplets that start with the same number of the cations, different temperature leads to different final charge states. As the temperature increases, the solvent evaporation rate also increases, thereby accelerating both solvent and ion evaporations. In MeCN droplets, the maximum charge state that PEG64 can sustain is +4 *e*, which has been obtained at a low temperature ($T = 250$ K). The higher charge state of PEG at the lower temperature may be attributed to the following three reasons: (1) the cations have a sufficient amount of time to interact with the macromolecule as solvent evaporation slows down, (2) the macromolecule does not become compact rapidly as its conformational dimension is strongly correlated to the size of the droplet (see Figure 7a), and (3) the surface tension of solvent generally decreases as temperature increases.

The difference in the final charge state from the case of water droplets is attributed to the different mechanisms of sodiation and ejection of the macromolecule. PEG64 on the surface of an aqueous droplet has an extended conformation that maximizes its access to the ions. On the other hand, PEG64 in a charged MeCN droplet becomes more compact as the droplet shrinks (Figure 7b), thus exposing less in the interactions with the ions. In MeCN, PEG is sodiated only when the cations diffuse close to the macromolecule while the parent droplet loses its mass and charge via evaporation. The charging of PEG in MeCN is different from that predicted by the CRM. The CRM states that during droplet evaporation, single charges are released from the droplet by Rayleigh's mechanism, and when the size of the droplet shrinks to the size close to that of the macro-ion, complete desolvation causes the remaining charges to collapse onto the surface of the macro-ion [17, 66]. However, we do not observe the adhesion of the ions onto compact PEG at the latest stage of desolvation; that is, ions can bind to PEG during the evolution of the droplet while solvated ions are released from the parent droplet. This behavior is consistent with our previous study on PEG in a charged MeOH droplet [33]. Therefore, one of the general and unsurprising findings of the comparison between the charging mechanisms of PEG in aqueous and MeCN droplets is that the solvent plays a pivotal role in the charging mechanism and the manner in which PEG64 emerges from a droplet.

The conformational changes of the flexible macromolecule residing in the interior of the droplet are significant as

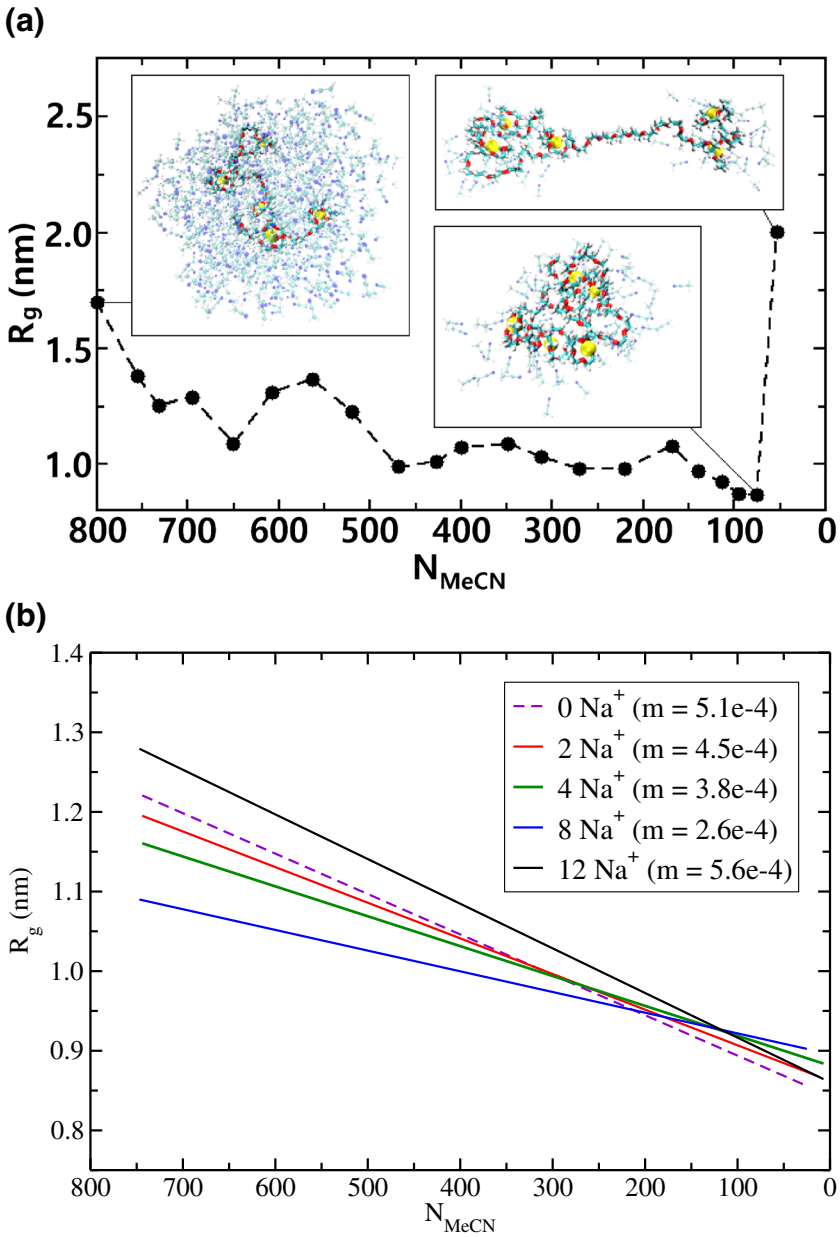

Figure 7. (**a**) R_g of PEG64-5Na^+ as a function of the number of remaining MeCN molecules (N_{MeCN}) in an evaporating droplet. The Na^+ ions coordinated by PEG64 are represented by yellow spheres. The entire evaporation process after relaxation occurs in approximately 7 ns at T = 280 K. (**b**) Declining trends of R_g of PEG64 in a MeCN droplet with different initial charges. The lines were obtained by fitting the points into a linear function. m is the slope of the lines

the droplet changes its size. To demonstrate this effect, we used the extreme case of PEG64 in its maximum charge state (PEG64-5Na^+). In the absence of solvent, PEG64-5Na^+ has a linear conformation [48], whereas in the presence of solvent, the macro-ion is compact. A typical plot of the R_g evolution of PEG64-5Na^+ versus remaining MeCN molecules in an evaporating droplet is shown in Figure 7a. In the same figure, typical snapshots of the change in the conformation of the sodiated PEG64 during solvent evaporation are also included. These trends are common, regardless of the amount of initial charges added into the droplet (Figure 7b).

The general behavior that is found by examining the stability of the sodiated PEG64 in MeCN droplets is that the macro-ion stays compact up to the late stages of solvent evaporation. A single solvation shell is sufficient to maintain a highly charged linear macro-ion compact. It is at the late stage of evaporation that it partially extends when a small amount of solvent is still present. Depending on the charge state of the macro-ion, the sodiated PEG bare of solvent will attain a conformation that may be linear or partially unwound [26].

We explain the stability of the highly charged compact PEG64 in small droplets by the Rayleigh limit (Equation 1), which is the critical value of the square of the charge-to-volume

ratio that a droplet becomes unstable. At a first glance, one would expect the Rayleigh limit to not hold for a small droplet that is mainly composed of the charged macromolecule.

However, we found that the partial extension of the macromolecule occurs close to the theoretical predictions of the Rayleigh limit (Table 1). In our estimates, we also considered the size of the macromolecule since it is a substantial part of the droplet. We approximated that each PEG monomer is equivalent to one MeCN molecule, and therefore, we used the experimental value of the surface tension for MeCN (29 mN/m) [67]. This approximation is valid as it is very close to the one used for the apparent surface energy of PEG globules [37]. Also Consta and Chung [26] characterized the conformational changes of PEG-$(Na^+)_n$ ions by using MD simulations, and they observed $Q_c \propto \sqrt{N}$ scaling behavior for the charged PEG (where Q_c is the critical charge and N is the degree of polymerization) as predicted by the experimental findings of Ude et al. [37] and the Rayleigh criterion. In order to make a fair comparison with the Rayleigh limit, however, we believe that we need to include the elastic energy of the chain in the Rayleigh expression. The manner to include the elastic energy of the polymer chain into a Rayleigh expression requires a separate investigation from the present study, and to our knowledge, this aspect is still to be examined. Here we note that the partial unwinding of the chain in the latest stage of desolvation has the features of the activated contiguous extrusion mechanism (A-CEM) [5, 28].

We also remark that the relationship between the gas-phase conformations of polymer ions and their charge states has been an important question to be addressed in mass spectrometry. For example, Criado-Hidalgo [68] has produced predominantly globular ions of large PEG chains with moderate charge states in negative ESI in order to facilitate ion identification in ion mobility separation coupled to mass spectrometry (IMS-MS). For the ions of small PEG chains (< 14 kDa) with charge state (+1 to +5 e), Ude et al. [37] formulated an approximate criterion for the critical mass (m^*) of PEG below which PEG globules lose stability at a Rayleigh-like limit: $m^*(z) \sim 500z^2$ where z is the charge state that values up to 5. This predicts that a PEG64 ion (≈2.8 kDa) adopts globular geometry only when it bears up to two Na^+ ions, which is consistent with our findings; we found that the conformational shapes of PEG64-zNa$^+$ are fully stretched when z = 4,5, partially stretched when z = 3, and compact when z = 1,2.

Table 1. Charge States and Droplet Sizes of MeCN Droplets

N_{sol} (with PEG64)	Charge state of PEG64 (e)	R.L. Charge (e)
57 (121)	+5	+4.0
20 (84)	+4	+3.3
5 (69)	+3	+3.0

The first column shows the number of solvent molecules in a droplet. In the estimate, we assumed that the 64 monomers of PEG are equivalent in size to 64 MeCN molecules. The sum of the solvent molecules and the equivalent PEG64 are shown in parenthesis. The second column shows the simulation-determined charge that a droplet can hold right before the release of charge. The third column shows the Rayleigh limit (R.L.) estimate of the charge that a droplet can hold

Mixture of Solvents PEG shows distinct behaviors of solvation and sodiation in pure water and MeCN droplets. Then, an interesting question may arise: What would happen if it is in a mixture of those two solvents? Solvation properties of a water/MeCN binary mixture have been widely studied. Particularly, it has been revealed that micro-heterogeneity in a binary solvent mixture may be displayed as the direct consequence of specific solvent–solvent interactions (e.g., water and some organic solvents such as MeCN [69–73] and dimethyl sulfoxide [72, 74]). In our simulations of H_2O/MeCN mixtures at various compositions, we confirmed the micro-heterogeneity of the binary mixture in a droplet by observing that the size of the water clusters grows as the aqueous component increases, which is consistent with the findings in Ref. [75]. Also, we found that the liquid/vapor interface of the droplet is more enriched in MeCN molecules, whereas water molecules are located mainly in the interior of the droplet. The water molecules are apt to be clustered with one another, many of which surround free and bound Na^+ ions on PEG. Therefore, the presence of solutes may promote the heterogeneous microstructure of the miscible binary solvent when they show preferential solvation by one solvent over the other. For example, the preferential hydration of Na^+ ions has been observed in bulk water/MeCN mixture [76–78], which is consistent with our simulations (Supplementary Table S2 in the Online Resource).

Interestingly, we found that micro-heterogeneous solvation, enhanced by the presence of the cations, in combination with differential evaporation rates of the two solvents, leads to the formation of the inner aqueous core at the point when the aqueous component becomes dominant. Figure S5 in the Online Resource shows that the water loss is in a linear trend, whereas the MeCN follows an exponential decay. The order of solvent depletion by evaporation, therefore, is clearly seen: MeCN disappears at a faster rate. The insets show water clusters moving closer to one another and aggregate as the droplet shrinks in size due to solvent evaporation. The formation of an aqueous core is critical in determining the final charge state of the macromolecule in these droplets of binary mixtures.

The formation of the water core is evidenced by the change in the chain dimension of PEG64 as solvent evaporates. In other words, the impact of solvent composition is reflected in the conformations of the macromolecule. As shown in the previous section, when a flexible linear macromolecule (even with a maximum charge state) is located inside a droplet (as for PEG64 in an MeCN droplet), the chain dimension becomes smaller as the size of the droplet decreases by solvent evaporation. When the aqueous component dominates (i.e., χ_{MeCN} = 0.2), as shown in Figure 8, the macromolecule is confined in the interior of the mixture droplet, and simultaneously confined on the surface of the aqueous core. This "sandwiched" solvation at the MeCN/water boundary due to early phase separation

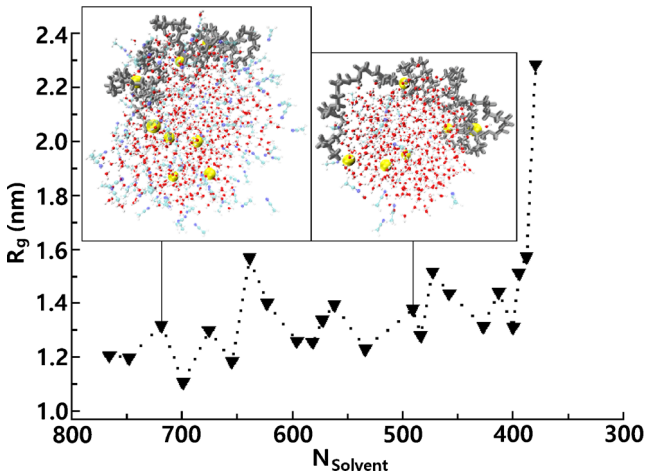

Figure 8. Radius of gyration of PEG64 (R_g) versus total number of solvent molecules present in the parent droplet ($N_{solvent}$) when χ_{MeCN} = 0.2 at T = 300 K. In snapshots, PEG64 is colored in gray for the purpose of better visualization

of the binary solvent mixture is a direct result of the solvent–solvent and solvent–polymer interactions in water and MeCN. However, the binary solvent mixture has differential evaporating rates for its components (see Figure S5 in the Online Resource), and thus, the conformational dimension of PEG64 is not affected by the depletion of MeCN. The sudden jump at the late stage arises from the partial extrusion of the macro-ion from the main droplet. On the contrary, when the MeCN component dominates (i.e., χ_{MeCN} = 0.8), the macromolecule is confined in the interior of the mixture droplet. However, because of the lack of the aqueous core at the initial stage, the degree of extension of PEG64 is largely affected by the droplet shrinkage due to the higher evaporation rate of the MeCN component, until the water component dominates by forming the aqueous core. As shown in Figure S6a in the Online Resource, there are two distinct regimes. The blue line represents the MeCN regime where the conformational size of the macromolecule is decreasing according to the solvent (mainly MeCN) evaporation. On the other hand, the red line represents the water regime where the chain dimension is kept almost the same due to the predominant presence of the water component along with its slower evaporating rate. When neither component predominates in number (i.e., χ_{MeCN} = 0.5), the two distinct regimes are still found as in χ_{MeCN} = 0.8. Yet, the range of the MeCN regime is shorter simply because a smaller amount of MeCN molecules are present (Figure S6b in the Online Resource).

As described in the previous section, PEG64 in charged single-component solvent droplets undergoes distinct solvation, sodiation, and release mechanisms, relying on the location of macromolecular solvation determined by PEG–solvent interactions. The final charge state of the macromolecule in the droplets of the binary mixture, therefore, may be sensitive to the solvent composition of the droplet. However, we found that the final charge state and the manner via which PEG emerges from the droplets can be identical to the case found in pure aqueous droplets. This is obvious in the regime of a higher aqueous component: the charge reduction at the critical limit is dominated by sequential partial releases of the macro-ion at the late stage. In the regime of a lower mole fraction of MeCN, a series of Coulomb fissions occur at the early stage as a predominant mechanism to eliminate excess charges from the parent droplet, and PEG64 is extruded in a sequential manner when only the small water droplet is left. As shown in Table 2, the number of charge-reducing events (Coulomb fissions versus macromolecular partial releases) before the complete detachment of PEG64 from the droplet is different, depending on the solvent compositions. Yet, the number of the cations remaining in the aqueous core is larger than or equal to four in all composition ratios, owing to the preferential hydration of the ions. In other words, even at the small mole fraction of water (i.e., χ_{MeCN} = 0.8), PEG64 can be liberated from the parent droplet through sequential partial releases as in a charged pure aqueous droplet, leading to the final charge state of +4 e. This is attributed to the formation of the inner water core in combination with preferential hydration of the cations.

Table 2. Number of Coulomb Fissions (N_{CF}), Number of Free Na^+ Ions before the First Partial Release of the Macro-Ion (N_{Na^+}), and Final Charge State of PEG64 in Different Solvent Compositions (χ_{MeCN})

χ_{MeCN}	N_{CF}	N_{Na^+}	Final charge state
0	0	8	PEG64-4Na^+
0.2	2	6	PEG64-4Na^+
0.5	2	6	PEG64-4Na^+
0.8	4	5	PEG64-4Na^+
1.0	5	3	PEG64-3Na^+

Conclusions

In electrospray ionization (ESI), the manners that a macromolecule emerges from charged nanodroplets have been described predominantly by the charge residue mechanism (CRM) [16, 17] and the ion evaporation mechanism (IEM) [18–20]. In the former mechanism, excess charge is reduced from the parent droplet at the critical level by a series of Coulomb fissions during the course of solvent evaporation. At the very late stage of the desolvation process, remaining ions collapse onto the macromolecule. It has been proposed, based on an ample body of experimental evidence [17, 20, 36, 79], that the distinction between these two mechanisms may be based on the molecular mass of an analyte: the CRM for massive, heavy macromolecules (such as globular protein complexes) and the IEM for small, light ions (including simple atomic and molecular ions). Here we have shown that this distinction contradicts our findings where the same macro-ion emerges from a droplet in different ways depending on its interactions with the solvent. Fenn et al. [36] argued that PEGs

leave the droplets via the IEM, based on his observations that lower charge states than a certain value were not detected in their mass spectra acquired from ESI experiments. We have provided the details of rather complicated mechanisms of the extrusion of the charged PEG from aqueous droplets and water/MeCN droplets. The extrusion mechanism is coupled to the charging of PEG, and we have called this mechanism the charging-induced extrusion mechanism (CI-EM). On the other hand, PEG64 in charged MeCN droplets resides in the interior of the droplet and becomes charged throughout solvent evaporation. The conventional IEM and CRM do not provide a crucial link between the nature of solvent and the releasing mechanism of a macromolecule. In this study, we emphasize the significant role of solvent not only to the solvation and sodiation properties, but also to the release mechanism of PEG64 as a representative to flexible linear macromolecules. In other words, the nature of solvent can grant complexity to solvent-ion-macromolecule interactions, which, in turn, determines the final ejection mechanism of a macromolecule, not only predicted by its molecular weight.

The role of surface tension in the determination of the final charge state of a macromolecule has been questioned in ESI experiments [80–86]. It has been found that higher charge states can be observed when the surface tension of the liquid rises, as the droplets can hold more charges that would be otherwise lost during droplet disintegrations at the early stage of the droplet evolution [87]. Also, Iavarone and Williams [88] demonstrated that in the absence of other factors, the surface tension of the droplet in the late desolvation process is a critical factor for overall analyte charge by investigating the extent of charging of different analytes, including PEGs, with ESI-MS. They used methanol and water as single-component solutions and added *m*-nitrobenzyl alcohol (*m*-NBA) to alter the surface tension of solvent. They found a strong correlation between the surface tension of solvent and the final charge state of the macro-ion. Even though there is still the ongoing debate on the role of surface tension (and its relevance to protein supercharging [86]), it seems that their experimental observations are consistent with our simulations of charged droplets of pristine water and acetonitrile. According to the Rayleigh mechanism, it is expected that the addition of an organic solvent with lower surface tension and lower volatility than water should lead to a lower charge distribution of analytes. However, our findings reveal that in addition to the surface tension of solvent, more factors come into play in the charging mechanism of the macromolecule. The difference in the charge state of PEG is attributed mainly to the combination of the location of PEG in a droplet (surface versus interior) and how rapidly the solvent evaporates. We found that PEG64 ends up with four Na^+ ions when solvated in water droplets, whereas it often takes less than four charges when solvated in acetonitrile droplets. This is because (1) PEG64 is on the surface of the water droplet, adopting more extended conformations, (2) the location of solvation of the macromolecule alters the manner that PEG is charged and released, and (3) more of the free Na^+ ions floating in acetonitrile droplets escape the parent droplet by Coulomb fissions due to its faster evaporation rate. Interestingly, however, experimental results countering the significance of surface tension have been provided [81–85]. Also, we found that the presence of MeCN in an aqueous droplet may not have a critical impact on the release mechanism and the final charge state of PEG64, at least for the three composition ratios we examined in this article (i.e., χ_{MeCN} = 0.2, 0.5, and 0.8), although the addition of MeCN into an aqueous solution is known to decrease the surface tension of the resulting mixture [89]. As PEG shows distinctive ejection mechanisms with varying final charge states based on the type of solvent, it was strongly expected that the macromolecule would be induced to have intermediate degrees of those properties, depending on the solvent composition ratio. However, our finding is completely different: the introduction of a MeCN component into a H_2O droplet does not change the charging and ejecting mechanisms, and therefore, PEG64 in these binary droplet systems shares the common features of the IEM. We attributed this to micro-heterogeneity, different solvent evaporation rates, and preferential hydration of Na^+ ions.

In order to study the effect of solvent on the maximum charge state and charge state distribution of proteins generated by ESI, Iavarone et al. [90] compared electrospray spectra of cytochrome *c* and myoglobin in the solution mixture of 47% water/50% organic solvent/3% acetic acid, where the organic component was methanol, MeCN, or isopropanol. They claimed that the charge state distributions of the two proteins shift to lower charge with a noticeable reduction in the abundance of the maximum charge state. Similarly, Hopper et al. [91] placed a small reservoir of MeCN into the atmospheric pressure region of an electrospray source, and they found that the average charge states of proteins (trypsin–benzamidine protein–inhibitor complex and human transthyretin) sprayed from aqueous buffers were lessened by exposing electrosprayed droplets to the neutral solvent vapor. According to their studies, the effect of MeCN molecules on the final charge state of a macromolecule is not negligible, whether they are present inside or outside the droplet, as they result in the decrease in the charge states of the macromolecular ion. This is apparently not in accord with our results because the cationization of PEGs is typically dominated by metal cation adduction [36, 88], whereas proteins have more complicated architectures and both covalent and non-covalent interactions that PEGs do not have. For instance, it has been commonly known that the charge state distribution of a protein ion is influenced significantly by its molecular conformation and acid-base chemistry, both in solution and in the gas phase [90]. Denatured, elongated protein structures are prone to have higher charge states than their folded tertiary structures because of higher affordability of the electrostatic repulsions between neighboring charges and higher accessibility of basic residues in the protein [90]. Also, the charge transfer between a protein and solvent molecules may involve proton transfers in addition to the adduction of a charged species. These aspects of proteins make it difficult to extend our findings to the case of protein ions generated by ESI.

Our study poses additional engaging questions to be asked. For example, the charging and release mechanisms of the flexible macromolecule may differ simply by

replacing Na^+ ions with other salt ions. It is of significance to answer if the nature of charge carriers (e.g., molecular ions such as guanidinium and tetramethylammonium ions versus simple metal ions such as sodium and calcium ions) has any striking impact on how a flexible macromolecule is released from the droplet. In particular, the size and the molecular geometry of charge carriers may affect the ionization mechanism of the macromolecule. For example, large, complex ions may require a longer sequence of monomers with complicated looping patterns when they charge the macromolecule, possibly reducing the final charge state of the macro-ion.

Acknowledgements

S.C. acknowledges the Discovery Grant of the Natural Sciences and Engineering Research Council of Canada (NSERC) and a Marie Curie International Incoming Fellowship (EC) held at the Department of Chemistry of the University of Cambridge, UK, for funding this research. The computing facilities provided by SciNet and SHARCNET are also acknowledged. M.I.O. acknowledges financial support from the Doctorate Scholarship from the University of Western Ontario and from the Alexander Graham Bell Canada Graduate Scholarships-Doctoral Program (CGS D) from NSERC. The authors thank Mr. Mahmoud Sharawy (graduate student, Department of Chemistry, University of Western Ontario) for a critical reading of the manuscript.

References

1. Podobnik, M., Savory, P., Rojko, N., Kisovec, M., Wood, N., Hambley, R., Pugh, J., Wallace, E.J., McNeill, L., Bruce, M., et al.: Crystal structure of an invertebrate cytolysin pore reveals unique properties and mechanism of assembly. Nat. Commun. **7**, 11598 (2016)
2. Schmidt, C., Beilsten-Edmands, V., Robinson, C.V.: Insights into eukaryotic translation initiation from mass spectrometry of macromolecular protein assemblies. J. Mol. Biol. **428**, 344–356 (2016)
3. Rayleigh, L.: XX. On the equilibrium of liquid conducting masses charged with electricity. Philos. Mag. **14**, 184–186 (1882)
4. Consta, S., Malevanets, A.: Disintegration mechanisms of charged nanodroplets: novel systems for applying methods of activated processes. Mol. Simul. **41**, 73–85 (2015)
5. Consta, S., Oh, M.I., Malevanets, A.: New mechanisms of macroion-induced disintegration of charged droplets. Chem. Phys. Lett. **663**, 1–12 (2016)
6. Hendricks, C., Schneider, J.: Stability of a conducting droplet under the influence of surface tension and electrostatic forces. Am. J. Phys. **31**, 450–453 (1963)
7. Richardson, C.; Pigg, A.; Hightower, R. On the stability limit of charged droplets. Proc. R.Soc. A **422**, 319–328 (1989)
8. Smith, J.N., Flagan, R.C., Beauchamp, J.: Droplet evaporation and discharge dynamics in electrospray ionization. J. Phys. Chem. A **106**, 9957–9967 (2002)
9. Grimm, R.L., Beauchamp, J.L.: Evaporation and discharge dynamics of highly charged droplets of heptane, octane, and p-Xylene generated by electrospray ionization. Anal. Chem. **74**, 6291–6297 (2002)
10. Schweizer, J.W., Hanson, D.: Stability limit of charged drops. J. Colloid Interface Sci. **35**, 417–423 (1971)
11. Gomez, A., Tang, K.: Charge and fission of droplets in electrostatic sprays. Phys. Fluids **6**, 404–414 (1994)
12. Taflin, D.C., Ward, T.L., Davis, E.J.: Electrified droplet fission and the Rayleigh limit. Langmuir **5**, 376–384 (1989)
13. Li, K.-Y., Tu, H., Ray, A.K.: Charge limits on droplets during evaporation. Langmuir **21**, 3786–3794 (2005)
14. Sharawy, M., Consta, S.: How do non-covalent complexes dissociate in droplets? A case study of the desolvation of dsDNA from a charged aqueous nanodrop. Phys. Chem. Chem. Phys. **17**, 25550–25562 (2015)
15. Sharawy, M., Consta, S.: Characterization of "Star" droplet morphologies induced by charged macromolecules. J. Phys. Chem. A (2016)
16. Dole, M., Mack, L.L., Hines, R.L., Mobley, R.C., Ferguson, L.D., Alice, M.B.: Molecular beams of macroions. J. Chem. Phys. **49**, 2240–2249 (1968)
17. dela Mora, J.F.: Electrospray ionization of large multiply charged species proceeds via Dole's charged residue mechanism. Anal. Chim. Acta **406**, 93–104 (2000)
18. Iribarne, J., Thomson, B.: Evaporation of small ions from charged droplets. J. Chem. Phys. **64**, 2287–2294 (1976)
19. Thomson, B., Iribarne, J.: Field-induced ion evaporation from liquid surfaces at atmospheric-pressure. J. Chem. Phys. **71**, 4451–4463 (1979)
20. Nguyen, S., Fenn, J.B.: Gas-phase ions of solute species from charged droplets of solutions. Proc. Natl. Acad. Sci. U.S.A. **104**, 1111–1117 (2007)
21. Hogan Jr., C.J., Carroll, J.A., Rohrs, H.W., Biswas, P., Gross, M.L.: Combined charged residue-field emission model of macromolecular electrospray ionization. Anal. Chem. **81**, 369–377 (2009)
22. Hogan Jr., C.J., Carroll, J.A., Rohrs, H.W., Biswas, P., Gross, M.L.: Charge carrier field emission determines the number of charges on native state proteins in electrospray ionization. J. Am. Chem. Soc. **130**, 6926–6927 (2008)
23. Steinberg, M.Z., Breuker, K., Elber, R., Gerber, R.B.: The dynamics of water evaporation from partially solvated cytochrome c in the gas phase. Phys. Chem. Chem. Phys. **9**, 4690–4697 (2007)
24. Patriksson, A., Marklund, E., van der Spoel, D.: Protein structures under electrospray conditions. Biochemistry **46**, 933–945 (2007)
25. Consta, S.: Manifestation of rayleigh instability in droplets containing multiply charged macroions. J. Phys. Chem. B **114**, 5263–5268 (2010)
26. Consta, S., Chung, J.K.: Charge-induced conformational changes of PEG-(Na(+))(n) in a vacuum and aqueous nanodroplets. J. Phys. Chem. B **115**, 10447–10455 (2011)
27. Chung, J.K., Consta, S.: Release mechanisms of poly(ethylene glycol) macroions from aqueous charged nanodroplets. J. Phys. Chem. B **116**, 5777–5785 (2012)
28. Consta, S., Malevanets, A.: Manifestations of charge induced instability in droplets effected by charged macromolecules. Phys. Rev. Lett. **109**, 148301 (2012)
29. Ahadi, E., Konermann, L.: Modeling the behavior of coarse-grained polymer chains in charged water droplets: implications for the mechanism of electrospray ionization. J. Phys. Chem. B **116**, 104–112 (2012)
30. Konermann, L., Rodriguez, A.D., Liu, J.: On the formation of highly charged gaseous ions from unfolded proteins by electrospray ionization. Anal. Chem. **84**, 6798–6804 (2012)
31. Nohmi, T., Fenn, J.: Electrospray mass spectrometry of poly(ethylene glycols) with molecular weights up to five million. J. Am. Chem. Soc. **114**, 3241–3246 (1992)
32. Fenn, J. B., Rosell, J., Nohmi, T., Shen, S., Banks, F.J.: Electrospray ion formation: desorption versus desertion. ACS Sym. Ser. **619**, 60–80 (1996)
33. Soltani, S., Oh, M., Consta, S.: Effect of solvent on the charging mechanisms of poly(ethylene glycol) in droplets. J. Chem. Phys. **142**, 114307 (2015)
34. Kienberger, F., Pastushenko, V.P., Kada, G., Gruber, H.J., Riener, C., Schindler, H., Hinterdorfer, P.: Static and dynamical properties of single poly(Ethylene Glycol) molecules investigated by force spectroscopy. Single Mol. **1**, 123–128 (2000)
35. Lee, H., Venable, R.M., MacKerell, A.D., Pastor, R.W.: Molecular dynamics studies of polyethylene oxide and polyethylene glycol: hydrodynamic radius and shape anisotropy. Biophys. J. **95**, 1590–1599 (2008)
36. Wong, S.F., Meng, C.K., Fenn, J.B.: Multlple charging in electrospray ionization of poly(ethylene glycols). J. Chem. Phys. **92**, 546–550 (1988)
37. Ude, S., dela Mora, J.F., Thomson, B.A.: Charge-induced unfolding of multiply charged polyethylene glycol ions. J. Am. Chem. Soc. **126**, 12184–12190 (2004)

38. Larriba, C., dela Mora, J.F.: The gas phase structure of coulombically stretched polyethylene glycol ions. J. Phys. Chem. B **116**, 593–598 (2012)
39. Bogan, M.J., Agnes, G.R.: Poly (ethylene glycol) doubly and singly cationized by different alkali metal ions: Relative cation affinities and cation-dependent resolution in a quadrupole ion trap mass spectrometer. J. Am. Soc. Mass Spectrom. **13**, 177–186 (2002)
40. von Helden, G., Wyttenbach, T., Bowers, M.T.: Conformation of macromolecules in the gas phase: use of matrix-assisted laser desorption methods in ion chromatography. Science **267**, 1483 (1995)
41. Gidden, J., Wyttenbach, T., Jackson, A.T., Scrivens, J.H., Bowers, M.T.: Gas-phase conformations of synthetic polymers: poly (ethylene glycol), poly (propylene glycol), and poly (tetramethylene glycol). J. Am. Chem. Soc. **122**, 4692–4699 (2000)
42. Chandrasekhar, J., Spellmeyer, D.C., Jorgensen, W.L.: Energy component analysis for dilute aqueous-solutions of Li+, Na+, F-, and Cl- ions. J. Am. Chem. Soc. **106**, 903–910 (1984)
43. Jorgensen, W.L., Tirado-Rives, J.: The OPLS Force Field for Proteins. Energy Minimizations for Crystals of Cyclic Peptides and Crambin. J. Am. Chem. Soc **110**, 1657–1666 (1988)
44. Jorgensen, W.L., Chandrasekhar, J., Madura, J.D., Impey, R.W., Klein, M.L.: Comparison of simple potential functions for simulating liquid water. J. Chem. Phys. **79**, 926–935 (1983)
45. Lindahl, E., Hess, B., van der Spoel, D.: GROMACS 3.0: A package for molecular simulation and trajectory analysis. J. Mol. Mod **7**, 306–317 (2001)
46. Humphrey, W., Dalke, A., Schulten, K.J.: Molec. Graphics. **14**(1), 33–38 (1996)
47. O'Neil, M. J.: The Merck index: An encyclopedia of chemicals, drugs, and biologicals.Whitehouse Station, Merck (2006)
48. Sharawy, M., Consta, S.: Effect of counterions on the charging mechanisms of a macromolecule in aqueous nanodrops. J. Chem. Phys. **141**, 104321 (2014)
49. Prasitnok, K., Wilson, M.R.: A coarse-grained model for polyethylene glycol in bulk water and at a water/air interface. Phys. Chem. Chem. Phys. **15**, 17093–17104 (2013)
50. Zhou, P., Brown, W.: Static and dynamic properties of poly(ethylene oxide) in methanol. Macromolecules **23**, 1131–1139 (1990)
51. Hakem, I.F., Lal, J.: Polyelectrolyte-like behaviour of poly(ethyleneoxide) solutions with added monovalent salt. Europhys. Lett. **64**, 204 (2003)
52. Cifra, P., Benková, Z., Bleha, T.: Persistence lengths and structure factors of wormlike polymers under confinement. J. Phys. Chem. B **112**, 1367–1375 (2008)
53. Shin, J., Cherstvy, A.G., Metzler, R.: Kinetics of polymer looping with macromolecular crowding: effects of volume fraction and crowder size. Soft Matter **11**, 472–488 (2015)
54. Shin, J., Cherstvy, A.G., Metzler, R.: Polymer looping is controlled by macromolecular crowding, spatial confinement, and chain stiffness. ACS Macro Lett. **4**, 202–206 (2015)
55. Cifra, P., Benkova, Z., Bleha, T.: Effect of confinement on properties of stiff biological macromolecules. Faraday Discuss. **139**, 377–392 (2008)
56. Cifra, P., Bleha, T.: Simulation of chain organization in encapsulated polymers. Macromol. Symp. **296**, 336–341 (2010)
57. Morrison, G., Thirumalai, D.: Semiflexible chains in confined spaces. Phys. Rev. E **79**, 011924 (2009)
58. Cerdà, J.J., Chakrabarti, A., Sintes, T.: Excluded volume effects on polymer chains confined to spherical surfaces. Macromolecules **38**, 1469–1477 (2005)
59. Spakowitz, A.J., Wang, Z.-G.: Semiflexible polymer confined to a spherical surface. Phys. Rev. Lett. **91**, 166102 (2003)
60. Consta, S., Malevanets, A.: Classification of the ejection mechanisms of charged macromolecules from liquid droplets. J. Chem. Phys. **138**, 044314 (2013)
61. Hezaveh, S., Samanta, S., Milano, G., Roccatano, D.: Structure and dynamics of 1,2-dimethoxyethane and 1,2-dimethoxypropane in aqueous and non-aqueous solutions: A molecular dynamics study. J. Chem. Phys. **135**, 164501 (2011)
62. Hezaveh, S., Samanta, S., Milano, G., Roccatano, D.: Molecular dynamics simulation study of solvent effects on conformation and dynamics of polyethylene oxide and polypropylene oxide chains in water and in common organic solvents. J. Chem. Phys. **136**, 124901 (2012)
63. Kim, M.: W. Surface activity and property of polyethyleneoxide (PEO) in water. Colloids Surf. Acsa **128**, 145–154 (1997)
64. Israelachvili, J.: The different faces of poly(ethylene-glycol). Proc. Natl. Acad. Sci. U.S.A. **94**, 8378–8379 (1997)
65. Chingin, K., Frankevich, V., Balabin, R.M., Barylyuk, K., Chen, H., Wang, R., Zenobi, R.: Direct access to isolated biomolecules under ambient conditions. Angew. Chem. Int. Ed. Engl. **49**, 2358–2361 (2010)
66. Nasibulin, A.G., de la Mora, J.F., Kauppinent, E.I.: Ion-induced nucleation of dibutyl phthalate vapors on spherical and nonspherical singly and multiply charged polyethylene glycol ions. J. Phys. Chem. A **112**, 1133–1138 (2008)
67. Korosi, G., Kovats, E.S.: Density and surface tension of 83 organic liquids. J. Chem. Eng. Data **26**, 323–332 (1981)
68. Criado-Hidalgo, E., Fernández-García, J., de la Mora, F.J.: Mass and Charge Distribution Analysis in Negative Electrosprays of Large Polyethylene Glycol Chains by Ion Mobility Mass Spectrometry. Anal. Chem. **85**, 2710–2716 (2013)
69. Marcus, Y.: The structure of and interactions in binary acetonitrile + water mixtures. J. Phys. Org. Chem. **25**, 1072–1085 (2012)
70. Mountain, R.D.: Microstructure and hydrogen bonding in water-acetonitrile mixtures. J. Phys. Chem. B **114**, 16460–16464 (2010)
71. Oldiges, C., Wittler, K., Tonsing, T., Alijah, A.: MD calculated structural properties of clusters in liquid acetonitrile/water mixtures with various contents of acetonitrile. J. Phys. Chem. A **106**, 7147–7154 (2002)
72. Shin, D.N., Wijnen, J.W., Engberts, J.B., Wakisaka, A.: On the origin of microheterogeneity: mass spectrometric studies of acetonitrile-water and dimethyl sulfoxide-water binary mixtures (Part 2). J. Phys. Chem. B **106**, 6014–6020 (2002)
73. Takamuku, T., Tabata, M., Yamaguchi, A., Nishimoto, J., Kumamoto, M., Wakita, H., Yamaguchi, T.: Liquid structure of acetonitrile-water mixtures by x-ray diffraction and infrared spectroscopy. J. Phys. Chem. B **102**, 8880–8888 (1998)
74. Shin, D.N., Wijnen, J.W., Engberts, J.B., Wakisaka, A.: On the origin of microheterogeneity: a mass spectrometric study of dimethyl sulfoxide-water binary mixture. J. Phys. Chem. B **105**, 6759–6762 (2001)
75. Cringus, D., Yeremenko, S., Pshenichnikov, M.S., Wiersma, D.A.: Hydrogen bonding and vibrational energy relaxation in water-acetonitrile mixtures. J. Phys. Chem. B **108**, 10376–10387 (2004)
76. Marcus, Y.: Preferential solvation of ions in mixed solvents. Part 2.-The solvent composition near the ion. J. Chem. Soc., Faraday Trans. 1 **84**, 1465–1473 (1988)
77. Stellnberger, K.-H., Gritzner, G., Lewandowski, A., Orlik, M.: Thermodynamic transfer properties for Na+, Tl+ and Ag+ to water-acetonitrile mixtures. J. Chem. Soc. Faraday Trans. **91**, 875–880 (1995)
78. Covington, A.K., Dunn, M.: Nuclear magnetic resonance studies of preferential solvation. Part 7.-Sodium iodide in ethylene glycol-acetonitrile and in propylene glycol-acetonitrile mixtures. J. Chem. Soc., Faraday Trans. 1 **85**, 2835–2846 (1989)
79. Kebarle, P., Verkerk, U.H.: Electrospray: from ions in solution to ions in the gas phase, what we know now. Mass Spectrom. Rev. **28**, 898–917 (2009)
80. Sterling, H.J., Williams, E.R.: Origin of supercharging in electrospray ionization of noncovalent complexes from aqueous solution. J. Am. Soc. Mass Spectrom. **20**, 1933–1943 (2009)
81. Šamalikova, M., Grandori, R.: Protein charge-state distributions in electrospray-ionization mass spectrometry do not appear to be limited by the surface tension of the solvent. J. Am. Chem. Soc. **125**, 13352–13353 (2003)
82. Brahim, B., Alves, S., Cole, R.B., Tabet, J.-C.: Charge enhancement of single-stranded DNA in negative electrospray ionization using the supercharging reagent meta-nitrobenzyl alcohol. J. Am. Soc. Mass Spectrom. **24**, 1988–1996 (2013)
83. Šamalikova, M., Grandori, R.: Testing the role of solvent surface tension in protein ionization by electrospray. J. Mass Spectrom. **40**, 503–510 (2005)
84. Lomeli, S.H., Yin, S., Ogorzalek Loo, R.R., Loo, J.A.: Increasing charge while preserving noncovalent protein complexes for ESI-MS. J. Am. Soc. Mass Spectrom. **20**, 593–596 (2009)
85. Lomeli, S.H., Peng, I.X., Yin, S., Ogorzalek Loo, R.R., Loo, J.A.: New reagents for increasing ESI multiple charging of proteins and protein complexes. J. Am. Soc. Mass Spectrom. **21**, 127–131 (2010)
86. Ogorzalek Loo, R.R., Lakshmanan, R., Loo, J.A.: What protein charging (and Supercharging) reveal about the mechanism of electrospray ionization. J. Am. Soc. Mass Spectrom. **25**, 1675–1693 (2014)

87. Nguyen, H.P., Schug, K.A.: The advantages of ESI-MS detection in conjunction with HILIC mode separations: Fundamentals and applications. J. Sep. Sci. **31**, 1465–1480 (2008)
88. Iavarone, A.T., Williams, E.R.: Mechanism of charging and supercharging molecules in electrospray ionization. J. Am. Chem. Soc. **125**, 2319–2327 (2003)
89. Maximino, R.B.: Surface tension and density of binary mixtures of monoalcohols, water and acetonitrile: equation of correlation of the surface tension. Phys. Chem. Liq. **47**, 475–486 (2009)
90. Iavarone, A.T., Jurchen, J.C., Williams, E.R.: Effects of solvent on the maximum charge state and charge state distribution of protein ions produced by electrospray ionization. J. Am. Soc. Mass Spectrom. **11**, 976–985 (2000)
91. Hopper, J.T., Sokratous, K., Oldham, N.J.: Charge state and adduct reduction in electrospray ionization-mass spectrometry using solvent vapor exposure. Anal. Biochem. **421**, 788–790 (2012)